Available online at www.sciencedirect.com
ScienceDirect
Journal of Power Sources 180 (2008) 92–102
JOURNAL OF POWER SOURCES
www.elsevier.com/locate/jpowsour

Measurement of oxygen chemical potential in thin electrolyte film, anode-supported solid oxide fuel cells

Hyung-Tae Lim, Anil V. Virkar *

Department of Materials Science & Engineering, 122 South Central Campus Drive, Salt Lake City, UT 84112, United States

Received 26 December 2007; received in revised form 29 January 2008; accepted 31 January 2008
Available online 8 February 2008

Abstract

Thin (~30–45 μm) gadolinia-doped ceria (GDC) electrolyte, Ni + yttria-stabilized zirconia (YSZ) anode-supported cells were fabricated with platinum reference electrodes (probes) embedded within the electrolyte layer. The exposed parts of the probes were sealed off from the atmosphere using an oxygen impermeable glass. Thus, no oxygen exchange could occur and voltage measurements at the probes correspond to the reduced negative electrochemical potential of electrons ($\varphi = -\tilde{\mu}_e/e$, where $\tilde{\mu}_e$ is the electrochemical potential of electrons and e is the electronic charge). The φ was measured at 650 °C under open circuit conditions with air circulated past the cathode and hydrogen circulated past the anode. The open circuit voltage was ~0.84 V. The voltages between the anode and reference electrodes were very small—less than 30 mV. This was attributed to significant electronic conduction throughout the electrolyte from anode/electrolyte interface to cathode/electrolyte interface. Thus, voltage drop mainly occurs across the cathode/electrolyte interface. The variation of chemical potential of oxygen, μ_{O_2}, within the GDC electrolyte was estimated, which showed a large drop in μ_{O_2} across the cathode/electrolyte interface. The oxygen partial pressure in GDC just inside the cathode was estimated to be $\sim 10^{-22}$ atm. Thus, in GDC-based anode-supported cells the effective electrolyte thickness is very small.

Keywords: Solid oxide fuel cells; Anode-supported; Chemical potential; Reference electrodes; Gadolinia-doped ceria

1. Introduction

1.1. Transport, local equilibrium and ionic and electronic currents

Numerous studies on transport through ionic conductors have been reported over the years. Oxygen ion conductors have been of particular interest due to their applications in such devices as solid oxide fuel cells (SOFCs), oxygen separators, and electrolyzers. The materials studied include those exhibiting predominantly ionic conduction (transference number >0.99) and those exhibiting significant electronic transport in addition to ion transport (mixed ionic and electronic conduction (MIEC)). Yttria-stabilized zirconia (YSZ) is essentially a pure oxygen ion conductor, while rare earth oxide-doped ceria exhibits mixed ionic and electronic conduction. The basis of the transport theory was developed over 50 years ago [1–3]. Virtually all reported studies on solid-state transport through ionic and mixed ionic-electronic conductors are based on two assumptions [4–6]:

(1) Transport of a charged species occurs down its electrochemical potential gradient, namely

$$j_i = -C_i B_i \nabla \tilde{\mu}_i \tag{1}$$

where C_i is the concentration of species i; $B_i = D_i/k_B T$ = mobility of species i, where D_i = diffusivity of species i; $\tilde{\mu}_i$ is the electrochemical potential of species i.

The corresponding current density due to species i is given by

$$I_i = -\frac{\sigma_i}{z_i e} \nabla \tilde{\mu}_i \tag{2}$$

where σ_i is the conductivity due to species i and z_i is the valence of species i.

(2) Local equilibrium exists everywhere in the system which allows one to write all transport equations in terms of gradients in chemical potentials of neutral species and electric potentials (electrochemical potential of electrons, $\tilde{\mu}_e$, or

* Corresponding author. Tel.: +1 801 581 5396; fax: +1 801 581 4816.
E-mail address: anil.virkar@m.cc.utah.edu (A.V. Virkar).

0378-7753/$ – see front matter © 2008 Published by Elsevier B.V.
doi:10.1016/j.jpowsour.2008.01.068

Nomenclature

B_i	mobility of species i (velocity/unit force)
C_i	concentration of species i
D_i	diffusivity of species i ($cm^2\ s^{-1}$ or $m^2\ s^{-1}$)
e	electronic charge (Coulombs)
E	Nernst voltage (V)
E_M	open circuit voltage (V)
E^a	internal EMF across anode/electrolyte interface in the equivalent circuit (V)
E^c	internal EMF across cathode/electrolyte interface in the equivalent circuit (V)
E^{el}	internal EMF across electrolyte (just inside interfaces) in the equivalent circuit (V)
V	cell voltage (V)
r_i^a	anode/electrolyte interfacial ionic area-specific resistance ($\Omega\,cm^2$)
r_i^c	cathode/electrolyte interfacial ionic area-specific resistance ($\Omega\,cm^2$)
r_i^{el}	electrolyte area-specific ionic resistance ($\Omega\,cm^2$)
r_e^a	anode/electrolyte interfacial electronic area-specific resistance ($\Omega\,cm^2$)
r_e^c	cathode/electrolyte interfacial electronic area-specific resistance ($\Omega\,cm^2$)
$R_i = r_i^c + r_i^{el} + r_i^a$	cell area-specific ionic resistance ($\Omega\,cm^2$)
$R_e = r_e^c + r_e^{el} + r_e^a$	cell area-specific electronic resistance ($\Omega\,cm^2$)
I_e	electronic current density through the membrane ($A\,cm^{-2}$)
I_i	ionic current density through the membrane ($A\,cm^{-2}$)
I_L	measured current density ($A\,cm^{-2}$)
k_B	Boltzmann constant ($J\,deg^{-1}$)
p_{O_2}	oxygen partial pressure (atm)
R	ideal gas constant ($J\,deg^{-1}\,mol^{-1}$)
R_L	load ($\Omega\,cm^2$)

Greek symbols

μ_i	chemical potential of species i ($J\,mol^{-1}$ or J/species)
$\tilde{\mu}_i$	electrochemical potential of species i ($J\,mol^{-1}$ or J/species)
$\varphi = -\tilde{\mu}_e/e$	reduced negative electrochemical potential of electrons (V)

negative reduced electrochemical potential of electrons, $\varphi = -\tilde{\mu}_e/e$, which is also the reduced electrochemical potential of electron holes). For a cation with valence z_1 ($z_1 > 0$), namely M^{z_1}, the local equilibrium is described by [2]:

$$M^{z_1} + z_1 e \Leftrightarrow M \tag{3}$$

which gives

$$\tilde{\mu}_{M^{z_1}} + z_1\tilde{\mu}_e = \mu_M = \tilde{\mu}_{M^{z_1}} - z_1 e\varphi \tag{4}$$

where μ_M is the chemical potential of neutral M. Similarly, for an anion of valence z_2 (or $-|z_2|$ since $z_2 < 0$), namely X^{z_2} or $X^{-|z_2|}$, local equilibrium is described by [2]:

$$X + |z_2|e = \tfrac{1}{2}X_2 + |z_2|e \Leftrightarrow X^{-|z_2|} \tag{5}$$

which gives

$$\mu_X + |z_2|\tilde{\mu}_e = \tfrac{1}{2}\mu_{X_2} + |z_2|\tilde{\mu}_e = \tilde{\mu}_{X^{-|z_2|}} = \tfrac{1}{2}\mu_{X_2} + z_2 e\varphi = \tfrac{1}{2}\mu_{X_2} - |z_2|e\varphi \tag{6}$$

where μ_X is the chemical potential of neutral X and μ_{X_2} is the chemical potential of neutral X_2.

These assumptions are universally made, either explicitly or implicitly in the reported studies on solid-state transport through ionic and MIEC conductors. Local equilibrium also implies that any changes in thermodynamic potentials from the equilibrium value occur such that [7]

$$\delta\tilde{\mu}_{M^{z_1}} + z_1\delta\tilde{\mu}_e = \delta\mu_M = \delta\tilde{\mu}_{M^{z_1}} - z_1 e\delta\varphi \tag{7}$$

and

$$\delta\mu_X + |z_2|\,\delta\tilde{\mu}_e = \tfrac{1}{2}\delta\mu_{X_2} + |z_2|\,\delta\tilde{\mu}_e = \delta\tilde{\mu}_{X^{-|z_2|}} = \tfrac{1}{2}\delta\mu_{X_2} - |z_2|e\,\delta\varphi \tag{8}$$

where $\delta\mu$ denotes a variation in the thermodynamic potential μ. The application of the local equilibrium concept to a predominantly ionic conductor has important implications concerning transport and chemical potentials (stability) [7].

The net current density due to all species is given by

$$I = \sum_i I_i = -\sum_i \frac{\sigma_i}{z_i e}\nabla\tilde{\mu}_i \tag{9}$$

assuming the electrodes can exchange all species (not blocking to any of the species). If for example the material is a predominantly ionic conductor, then current only due to ionic species dominates. That is, $I = I_{ion} + I_{elec} \cong I_{ion}$ since $|I_{ion}| \gg |I_{elec}|$. That is, in such a case, virtually all of the current is due to ionic species (typically one species) and transport of the remaining species can be ignored, insofar as the magnitude of the current is concerned. This, for example is the case with YSZ as the electrolyte in which the dominant current is due to oxygen ions. It is a common practice to equate all of the measured current with the ionic current through YSZ membranes.

An important point to note is that electronic current in a predominantly ionic conductor can be neglected only when considering the total current. However, insofar as the local equilibrium is concerned, electronic current cannot be neglected, no matter how small the electronic current is. This is because, the conditions described by Eqs. (7) and (8) can be satisfied only if electrons can be transported, in and out, so that variations in all thermodynamic potentials can occur under any applied or internal stimuli [7]. That is, the electronic conductivity cannot be set identically to zero or the electronic resistivity cannot be set to infinity. As has been shown previously this is because the electronic current enters the relations for the chemical potentials

of neutral species as a multiplicative factor (a product of electronic current and electronic resistance) [7–9]. For oxygen ion conductors, this means even in a predominantly ionic conductor such as YSZ, the electronic current cannot be neglected since it enters as a multiplicative factor (multiplication of the electronic current and the electronic resistance) in the equations for oxygen chemical potential, μ_{O_2}. Neglect of electronic current leads to indeterminacy of the chemical potentials of neutral species and violates the fundamental local equilibrium criterion [7,8]. The preceding implies that while the magnitude of the electronic current may be small (as an additive term in the total current), its effect on the chemical potential is multiplicative and can in fact dictate the very stability of the material under the given experimental or operating conditions.

1.2. Role of interfaces

The electrode/electrolyte interfaces are usually physically distinct, such as a sharp change in microstructure across an interface. Properties of the electrolyte in close proximity to the interface are different from those in the bulk electrolyte due to compositional variations (segregation of some species, and depletion of other species), space charge effects, etc. These regions can extend several nanometers into the electrolyte and in some cases even several microns. They may or may not be present in all materials. Even in the absence of such gradients (compositional, space charge), the electrolyte region very close to the interface must always exhibit different properties from the bulk. This is because atomic bond lengths of near surface atoms are different from those in the bulk due to unsatisfied bonds on the surface. For this reason, transport properties of interfacial regions must also always be different from those in the bulk. Since electronic conductivity of the bulk electrolyte cannot be identically zero for the aforementioned local equilibrium criterion, it means that electronic conduction must also occur through the interfacial regions. That is, interfacial regions must transport both ionic and electronic species, no matter how small is the current. Thus, the electrolyte for any modeling purposes must be divided into at least three separate regions: the two interfacial regions and the bulk.

When the two surfaces of a membrane are exposed to two different atmospheres, such as fuel and oxidant, the chemical potentials vary through the membrane—that is, they are functions of position. Since defect concentrations are functions of chemical potentials, the transport properties are also functions of position within the membrane. For this reason, the spatial variation of chemical potential is expected to be nonlinear. If the ionic and electronic transport properties are assumed to be independent of position, the spatial variation of chemical potentials is expected to be linear. As was discussed recently such an assumption only changes the details—but not the general features of transport [7]. In this manuscript, this assumption is made for illustration purposes only since it allows the use of simple equivalent circuits, such as the one shown in Fig. 1. The equivalent circuit shown in Fig. 1 ignores concentration polarization and activation polarization associated with the extended reaction zones in the porous electrodes [7,9]. The various parameters in the equivalent circuit are as follows: r_i^c, r_i^{el}, and r_i^a are ionic specific resistances of the cathode/electrolyte interface, electrolyte, and electrolyte/anode interface, respectively; r_e^c, r_e^{el}, and r_e^a are electronic-specific resistances of the cathode/electrolyte interface, electrolyte, and electrolyte/anode interface, respectively; and

$$E^c = \frac{\mu^I_{O_2} - \mu^c_{O_2}}{4e} \tag{10}$$

$$E^{el} = \frac{\mu^c_{O_2} - \mu^a_{O_2}}{4e} \tag{11}$$

and

$$E^a = \frac{\mu^a_{O_2} - \mu^{II}_{O_2}}{4e} \tag{12}$$

are the internal EMFs across the cathode/electrolyte interface, electrolyte, and electrolyte/anode interface, respectively, which are given in terms of the various oxygen chemical potentials, μ'_{O_2}s. The sum of the three corresponds to

$$E^c + E^{el} + E^a = \frac{\mu^I_{O_2} - \mu^{II}_{O_2}}{4e} = E \tag{13}$$

which is the Nernst voltage.

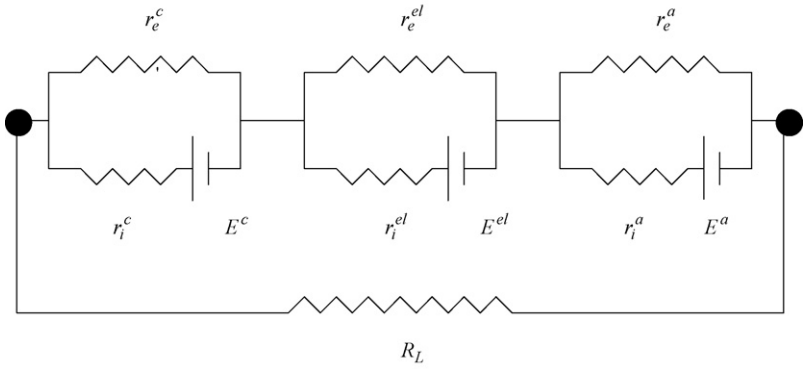

Fig. 1. A simplified equivalent circuit for an SOFC. The r_i's are the ionic resistances, r_e's are the electronic resistances, and E^α's are the internal EMF's (representing $\Delta\mu_{O_2}$'s). The circuit elements between the two filled circles are not physically separable and collectively represent the equivalent circuit. R_L denotes the external load. The open circuit condition is given by $R_L \to \infty$.

1.3. Ionic and electronic currents

For an SOFC with YSZ as the electrolyte, the electronic resistance is much greater than the ionic resistance. With reference to the equivalent circuit given in Fig. 1, this means $R_e = r_e^c + r_e^{el} + r_e^a \gg r_i^c + r_i^{el} + r_i^a = R_i$. Thus, the magnitude of the ionic current is much greater than the magnitude of the electronic current, that is, $|I_i| \gg |I_e|$, and the current measured in the external circuit $I_L = I_i + I_e$ is predominantly due to the ionic current through the membrane. The general equations of transport are given by [1–3]:

$$I_{O^{2-}} = I_i = \frac{\sigma_{O^{2-}}}{2e}\nabla\tilde{\mu}_{O^{2-}} = \frac{\sigma_{O^{2-}}}{4e}\nabla\mu_{O_2} - \sigma_{O^{2-}}\nabla\varphi \quad (14)$$

$$I_e = -\sigma_e \nabla\varphi \quad (15)$$

In terms of the various area specific resistances, the currents are given as follows:

Cathode/electrolyte interface (assuming a one-dimensional case, such that all potentials are functions of distance perpendicular to the electrolyte surface):

$$I^c_{O^{2-}} = -\frac{1}{4e}\frac{\mu^I_{O_2} - \mu^c_{O_2}}{r^c_i} + \frac{\varphi^I - \varphi^c}{r^c_i}, \quad I^c_e = \frac{\varphi^I - \varphi^c}{r^c_e} \quad (16)$$

Bulk electrolyte:

$$I^{el}_{O^{2-}} = -\frac{1}{4e}\frac{\mu^c_{O_2} - \mu^a_{O_2}}{r^{el}_i} + \frac{\varphi^c - \varphi^a}{r^{el}_i}, \quad I^{el}_e = \frac{\varphi^c - \varphi^a}{r^{el}} \quad (17)$$

Anode/electrolyte interface:

$$I^a_{O^{2-}} = -\frac{1}{4e}\frac{\mu^a_{O_2} - \mu^{II}_{O_2}}{r^a_i} + \frac{\varphi^a - \varphi^{II}}{r^a_i}, \quad I^a_e = \frac{\varphi^a - \varphi^{II}}{r^a_e} \quad (18)$$

In steady state, the divergence of ionic and electronic currents is individually zero, that is $\nabla \cdot I_{O^{2-}} = 0$ and $\nabla \cdot I_e = 0$, or $dI_{O^{2-}}/dx = 0$ and $dI_e/dx = 0$ in a one-dimensional case, which means the ionic current is constant (spatially independent) through all three regions, $I^c_{O^{2-}} = I^{el}_{O^{2-}} = I^a_{O^{2-}} = I_{O^{2-}} = I_i$; the electronic current is also constant through the three regions, $I^c_e = I^{el}_e = I^a_e = I_e$. Eqs. (16)–(18) can be rearranged to write the chemical potentials of oxygen just across the interfaces inside the electrolyte, namely $\mu^c_{O_2}$ and $\mu^a_{O_2}$ in terms of ionic and electronic currents [7,9].

$$\mu^c_{O_2} = \mu^I_{O_2} + 4e(r^c_i I_i - r^c_e I_e) \quad (19)$$

$$\mu^a_{O_2} = \mu^{II}_{O_2} - 4e(r^a_i I_i - r^a_e I_e) \quad (20)$$

Also, the rearrangement of equations for electronic transport gives

$$\varphi^c = \varphi^I - r^c_e I_e \quad (21)$$

$$\varphi^a = \varphi^{II} + r^a_e I_e \quad (22)$$

As a general rule, there should be abrupt changes in both μ_{O_2} and φ across both interfaces (since interfacial regions are very thin—on the order of nanometers, but with different properties than the bulk). Fig. 2 shows schematic variations of μ_{O_2} and φ through an SOFC. Relative values of transport properties (electrolyte and interfaces) can substantially influence the variations of μ_{O_2} and φ [7]. Also, if the transport properties of the electrolyte are functions of μ_{O_2}, then the variations of μ_{O_2} and φ through the electrolyte will be nonlinear (shown by broken lines in Fig. 2). In Ag_2S, for example, the variations of μ_{Ag} and φ are nonlinear [1].

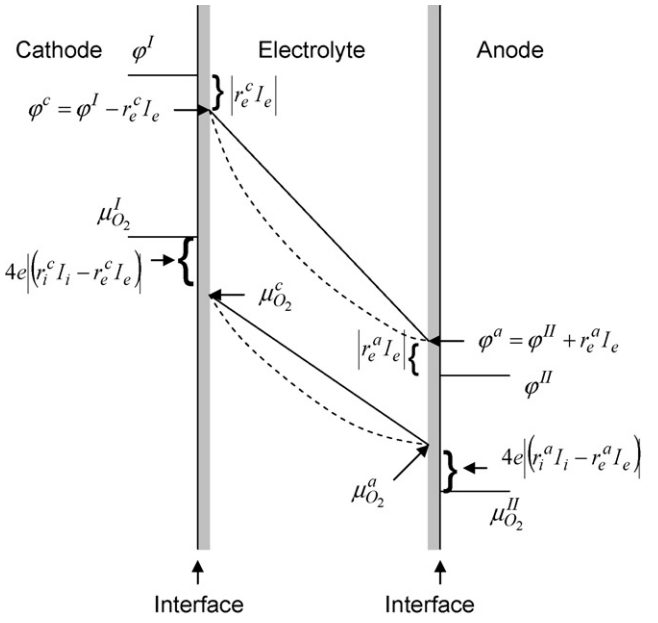

Fig. 2. Schematic variations of μ_{O_2} and φ across a membrane corresponding to the equivalent circuit in Fig. 1. If the transport properties of the membrane are dependent upon μ_{O_2} (and thus on position), the variations of μ_{O_2} and φ will be nonlinear (shown by broken lines).

1.4. Review of measurement of potentials using selective probes and calculations of potentials

Several studies have been reported on the estimation of thermodynamic potentials in solid-state ionic and mixed ionic electronic conductors [8,10–22]. Analysis of a selective probe for the measurement of φ and chemical potential of neutral silver in Ag_2S was first reported by Hebb [1]. Depending upon whether the tip of the probe can exchange electrons or silver ions, the measured voltage could be correlated with φ or μ_{Ag}. After this initial work by Hebb, several researchers have used the selective probe method. For example, the measurements of thermodynamic potentials in Ag|AgBr|Pt and Ag|AgBr||AgCl|Ag have been reported [19]. For the accurate measurement of μ_{Ag} in AgI, Pt probe shielded by an alumina tube has been used in one study so that only the tip contacted AgI [20]. For mixed ionic electronic conducting Cu_2O, MIEC probes have been used [10].

In cation conductors, as the ambient atmosphere does not contain the neutral metal corresponding to the cation, metal exchange with the atmosphere is generally not an issue. In anion conductors, especially oxygen ion conductors, interaction with oxygen in the ambient atmosphere must be taken into account. The concept of embedded reference electrodes has been

explored by Reed et al. [21]. In their studies, a Pt probe was embedded in an YSZ sample ~200 μm in thickness. However, it was not stated whether or not the probe was isolated from the atmosphere. An experimental study on the measurement of oxygen chemical potential, μ_{O_2}, on a thick gadolinia-doped ceria (GDC) sample has been reported by Mineshige et al. [22]. A 4-mm thick sample of GDC was exposed to fuel on one side and air on the other side at 1000 °C. After equilibration, the sample was sectioned and the μ_{O_2} profile was obtained using Raman spectroscopy [22]. Data were obtained in intervals ranging between ~50 μm and ~400 μm. The interval was ~400 μm near the anode and ~50 μm near the cathode. Several studies have been reported on theoretically estimating the μ_{O_2} variation within solid electrolytes [11–16]. However, in all of these studies it was assumed that the μ_{O_2} in the solid electrolyte in contact with the gas phase equilibrated across the interface. As has been shown recently, equilibration of μ_{O_2} across gas/solid interface cannot be assumed when the two surfaces of a solid are exposed to atmospheres containing different chemical potentials of oxygen, such as SOFC [7].

1.5. Measurement of reduced negative electrochemical potential of electrons, φ, by embedded reference electrodes

In the case of oxygen ion conductors, the probe should exchange only electrons and not oxygen in order to measure φ. Since the ambient atmosphere contains oxygen, it is necessary that the probe be completely isolated from the ambient. Fig. 3 shows a schematic of the experimental arrangement for the measurement of φ in a solid-state oxygen ion conducting electrolyte by embedding a platinum reference electrode. The exposed part of the probe is sealed off from the atmosphere using a glass which is impermeable to oxygen. Voltage is measured between a probe connected to one of the electrodes and the embedded probe. When the probes are equilibrated with the sample,

$$\tilde{\mu}_e(\text{Pt\#1}) = \tilde{\mu}_e^{x=0}(\text{electrode I}) \tag{23}$$

$$\tilde{\mu}_e(\text{Pt\#2}) = \tilde{\mu}_e^{x=x}(\text{embedded Pt}) \tag{24}$$

The voltage measured between the embedded probe and electrode I is given by [1]:

$$\Delta V = -\frac{\tilde{\mu}_e(\text{Pt\#2})}{e} + \frac{\tilde{\mu}_e(\text{Pt\#1})}{e} = -\frac{\tilde{\mu}_e^{x=x}(\text{embedded Pt})}{e} + \frac{\tilde{\mu}_e^{x=0}(\text{electrode I})}{e} = \varphi(x) - \varphi(0) = \Delta\varphi \tag{25}$$

Thus, using platinum wires and platinum reference electrodes embedded in the electrolyte, the reduced negative electrochemical potential of electrons (or reduced electrochemical potential of holes), $\varphi(x)$, can be measured. An important requirement is that the embedded probe should exchange only electrons and not oxygen.

1.6. Estimation of oxygen chemical potential within the electrolyte from the measurement of φ

Based on the criterion of local equilibrium, we have

$$\nabla\varphi = -\frac{1}{2e}\nabla\tilde{\mu}_{O^{2-}} + \frac{1}{4e}\nabla\mu_{O_2} \tag{26}$$

At open circuit, $I_i + I_e = 0$. If the electrolyte is a predominantly oxygen ion conductor (such as YSZ), at open circuit, $\nabla\tilde{\mu}_{O^{2-}} \cong 0$. Eq. (26) then reduces to

$$\nabla\varphi \cong \frac{1}{4e}\nabla\mu_{O_2} \tag{27}$$

Thus, gradient in μ_{O_2} can be readily obtained from the measurement of φ. At open circuit, from Eq. (27), the chemical potentials of oxygen just inside the electrolyte at the cathode and anode are given by

$$\mu_{O_2}^{c} \cong \mu_{O_2}^{I} - 4e(\varphi^{I} - \varphi^{c}) = \mu_{O_2}^{I} - 4er_e^{c}I_e = \mu_{O_2}^{I} + 4er_e^{c}I_i \tag{28}$$

$$\mu_{O_2}^{a} \cong \mu_{O_2}^{II} + 4e(\varphi^{a} - \varphi^{II}) = \mu_{O_2}^{II} + 4er_e^{a}I_e = \mu_{O_2}^{II} - 4er_e^{a}I_i \tag{29}$$

The corresponding oxygen partial pressures within the electrolyte just under the cathode and the anode are given,

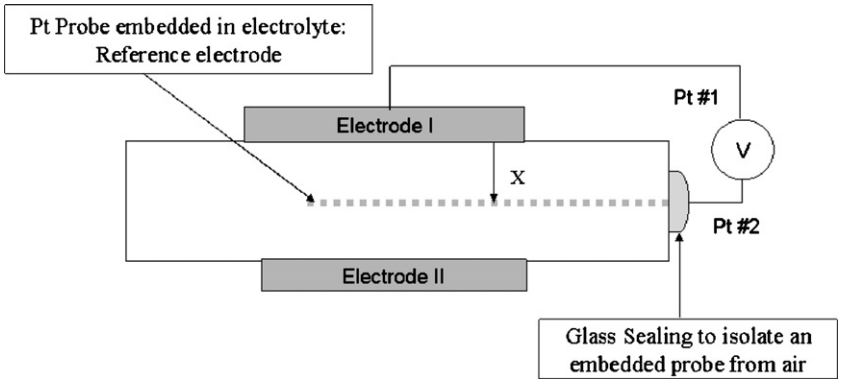

Fig. 3. A schematic showing an embedded reference electrode in a solid electrolyte membrane. The reference electrode (probe) is sealed off from the atmosphere using an oxygen impermeable glass.

respectively by

$$p^{c}_{O_2} \cong p^{I}_{O_2} \exp\left(-\frac{4e(\varphi^{I}-\varphi^{c})}{k_B T}\right) = p^{I}_{O_2} \exp\left(-\frac{4er^{c}_{e} I_e}{k_B T}\right) \quad (30)$$

$$p^{a}_{O_2} \cong p^{II}_{O_2} \exp\left(\frac{4e\left(\varphi^{a}-\varphi^{II}\right)}{k_B T}\right) = p^{II}_{O_2} \exp\left(\frac{4er^{a}_{e} I_e}{k_B T}\right) \quad (31)$$

In YSZ-based membranes, the electronic leakage is negligible. Thus, the net transport of oxygen from the cathode to the anode at open circuit is negligible, and Eqs. (28)–(31) can be used to estimate chemical potentials and partial pressures. Abrupt changes in both are expected at the two electrolyte/electrode interfaces, the magnitudes of these changes being dependent upon the relative values of transport parameters [7].

If the electrolyte exhibits significant electronic conduction (such as rare earth oxide-doped ceria), then $\nabla\tilde{\mu}_{O^{2-}} \neq 0$ even at open circuit and significant oxygen permeation may occur. In most ceria electrolyte-based SOFC operating between ~600 °C and 800 °C, the ionic transference number of the cell is typically ~0.8. The transference number of the membrane, including interfaces, is then given by

$$t_m = \frac{E_M}{E} = \frac{r^{c}_{e} + r^{el}_{e} + r^{a}_{e}}{r^{c}_{i} + r^{el}_{i} + r^{a}_{i} + r^{c}_{e} + r^{el}_{e} + r^{a}_{e}} = \frac{R_e}{R_i + R_e} \quad (32)$$

where

$$R_i = r^{c}_{i} + r^{el}_{i} + r^{a}_{i} \quad (33)$$

$$R_e = r^{c}_{e} + r^{el}_{e} + r^{a}_{e} \quad (34)$$

and E_M is the open circuit voltage.

At open circuit, the internal leakage current is given by

$$I_{leakage} = \frac{E}{R_i + R_e} = -I_i = I_e \quad (35)$$

As the internal leakage current is not negligible in ceria, it also means that $\nabla\tilde{\mu}_{O^{2-}} \neq 0$. The knowledge of $\nabla\tilde{\mu}_{O^{2-}}$ is required to estimate the chemical potentials within the electrolyte. Estimation of $\nabla\tilde{\mu}_{O^{2-}}$ requires the knowledge of r^{c}_{i}, r^{el}_{i}, and r^{a}_{i}. The average $\nabla\tilde{\mu}_{O^{2-}}$ (including interfaces) can be estimated from a cell performance test. It can be shown that the voltage vs. current density relation is given by

$$V = \frac{E R_e}{R_i + R_e} - \frac{R_i R_e}{R_i + R_e} I_L \quad (36)$$

Thus, from the slope and the intercept of this curve, both R_i and R_e can be obtained. The r^{el}_{i} for the electrolyte can be obtained using separate measurements involving electron blocking electrodes. It can be shown that the oxygen chemical potentials just inside the electrolyte at OCV are given by [7]:

$$\mu^{c}_{O_2} = \mu^{I}_{O_2} - 4e(r^{c}_{e} + r^{c}_{i})I_e = \mu^{I}_{O_2} + 4e(r^{c}_{e} + r^{c}_{i})I_i \quad (37)$$

$$\mu^{a}_{O_2} = \mu^{II}_{O_2} + 4e(r^{a}_{e} + r^{a}_{i})I_e = \mu^{II}_{O_2} - 4e(r^{a}_{e} + r^{a}_{i})I_i \quad (38)$$

The corresponding oxygen partial pressures within the electrolyte just under the electrodes are given by

$$p^{c}_{O_2} = p^{I}_{O_2} \exp\left(-\frac{4e(r^{c}_{i} + r^{c}_{e})(\varphi^{I}-\varphi^{c})}{r^{c}_{e} k_B T}\right) = p^{I}_{O_2} \exp\left(-\frac{4e(r^{c}_{i} + r^{c}_{e})I_e}{k_B T}\right) \quad (39)$$

$$p^{a}_{O_2} = p^{II}_{O_2} \exp\left(\frac{4e(r^{a}_{i} + r^{a}_{e})(\varphi^{a}-\varphi^{II})}{r^{a}_{e} k_B T}\right) = p^{II}_{O_2} \exp\left(\frac{4e(r^{a}_{i} + r^{a}_{e})I_e}{k_B T}\right) \quad (40)$$

The preceding shows that the knowledge of r^{c}_{i}, r^{a}_{i}, r^{c}_{e}, and r^{a}_{e} is necessary for estimating $\mu^{c}_{O_2}$ and $\mu^{a}_{O_2}$.

2. Experimental procedure

2.1. Cell fabrication

Anode-supported cells were fabricated using the following procedure. Powder mixture containing 70 wt.% NiO and 30 wt.% YSZ (composition: 8 mol% Y_2O_3–92 mol% ZrO_2) was made to which some carbon black was added to create porosity upon burn off. Additional porosity was created later in the anode upon reduction of NiO to Ni during cell testing. Discs of 3.3 cm in diameter and 1.5 mm in thickness were die-pressed and fired at 950 °C in air for 1 h. These discs were used as anode supports. A slurry containing 50 wt.% NiO and 50 wt.% GDC (composition: 20 mol% Gd_2O_3–80 mol% CeO_2) was prepared in butyl alcohol. Anode functional layer was applied using the NiO + GDC slurry on one side of each anode support disc by drop coating. The discs were again fired at 950 °C for 1 h. Then, the first electrolyte layer was drop coated using a slurry of GDC followed by firing at 1200 °C. Platinum paste was applied in the form of a thin and a very narrow strip over the electrolyte layer to form a reference electrode (Ref#2). The sample was heated to 950 °C to remove organics from the Pt paste. A second layer of GDC was drop coated to cover most of the surface except for a small part of the Pt strip, which was left exposed. The cell was again fired at 1200 °C. Another reference electrode (Ref#1) was similarly applied, followed by heating to 950 °C. Finally, one more layer of GDC was drop coated over most of the surface leaving small parts of both electrodes exposed. The cell was sintered at 1450 °C for 10 h. The total thickness of the GDC electrolyte was ~45 μm with the two reference electrodes positioned ~15 μm from the cathode/electrolyte and the anode/electrolyte interfaces, respectively. One cell was made with a total of three embedded reference electrodes; one (Ref#3) ~15 μm from anode/electrolyte interface, second (Ref#2) ~30 μm from anode/electrolyte interface, and third (Ref#1) ~38 μm from the anode/electrolyte interface. After sintering, cathode functional layer containing a mixture of LSC and GDC was applied followed by firing at 1100 °C. A layer of LSC was then applied

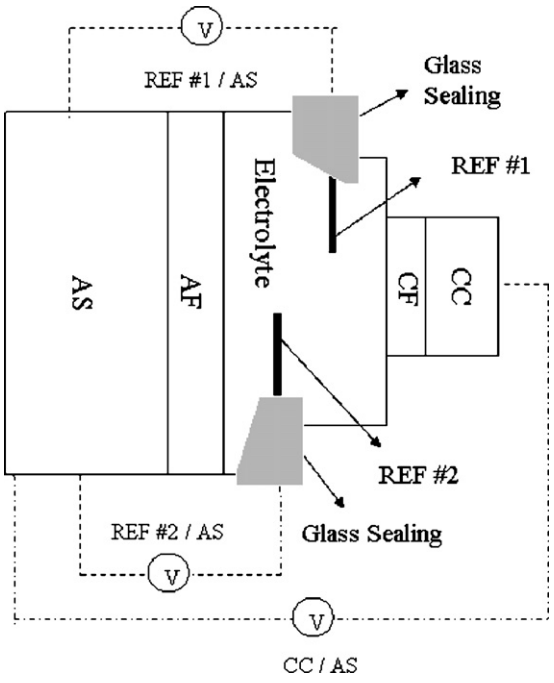

Fig. 4. A schematic of an anode-supported cell with embedded reference electrodes. The electrolyte thickness is shown exaggerated with respect to the anode support. AS, anode support; AF, anode functional layer or interlayer; CF, cathode functional layer or interlayer; CC, cathode current collector.

as a cathode current collector followed by again firing at 1100 °C. Pt wires were attached to the exposed parts of the embedded Pt probes. Exposed parts of the Pt reference electrodes were coated with a paste of sealing glass in ethylene glycol. The cell was fired at 850 °C to fuse the glass and isolate the exposed parts of the reference electrodes from air. This completes the cell fabrication procedure. Fig. 4 shows a schematic of the cell along with the position of reference electrodes. One cell was made with two embedded probes and a thin layer of YSZ on top of GDC to essentially block off electronic current. This cell was used to measure the Nernst voltage.

2.2. Cell testing

Cells with embedded Pt probes were tested using a specially designed fixture. The cell was secured at the end of an alumina tube with the anode facing the inside of the tube. Mica gasket was used as a glass-free seal. The cell was held in position by spring loading and was placed inside a tube furnace with the spring being outside the hot zone. The cell was then heated to 650 °C. A gas mixture containing 10% H_2 and balance nitrogen was circulated through the alumina tube over the anode surface to reduce NiO to Ni. Subsequently the anode gas was changed to ~100% H_2. Voltages between the anode and the reference electrodes, and between the anode and the cathode were measured under open circuit conditions. Voltage vs. current density polarization curve was measured on the cell with three embedded reference electrodes. OCV was measured on a cell with a thin YSZ coating over GDC.

2.3. Measurement of the conductivity of sealing glass

Three discs of YSZ were made by die-pressing followed by sintering. The surfaces of the discs were flat ground. A sandwich was formed using two of the discs with a layer of glass in between. The sample assembly was heated to 850 °C to fuse the glass. Platinum electrodes were applied on the surfaces of the sandwich sample as well as the remaining single disc. Two probe dc resistance measurements were made on the samples at 650 °C. From the difference of the two measurements, approximate value of the ionic conductivity of the glass was obtained.

2.4. Measurement of total conductivity of GDC in oxidizing and reducing atmospheres

A bar-shaped sample of GDC was fabricated by die-pressing a powder of GDC and sintering at 1450 °C. Platinum strips were painted on the bar in a four probe configuration. The sample was heated to 650 °C and its four probe dc resistance was measured. At 650 °C in air, the predominant transport is known to be by oxygen vacancies. Subsequently a gas mixture containing 10% H_2 + balance N_2 was introduced, which was later switched to ~100% H_2. The total resistance was measured as a function of time. Stable values in air and hydrogen were recorded as the resistances corresponding to the two atmospheres. From the sample dimensions, the corresponding resistivities were determined.

3. Results and discussion

3.1. Microstructures of cells with embedded electrodes

Fig. 5(a) and (b) are scanning electron micrographs (SEM) of a tested cell showing LSC + GDC cathode interlayer, the GDC electrolyte, and Ni + GDC anode interlayer. Also seen in the micrographs are the two embedded Pt electrodes, Reference#1 (close to the cathode) and reference#2 (close to the anode). The GDC electrolyte thickness is ~45 μm. Reference#1 and reference#2 are ~15 μm from the cathode/electrolyte interface and ~15 μm from the anode/electrolyte interface, respectively. Note that the GDC electrolyte appears to be fully dense with negligible porosity.

3.2. Measurement of the conductivity of the glass

Two probe dc resistance measurements were made at 650 °C on a YSZ disc with Pt electrodes and on the YSZ–glass–YSZ sandwich sample with Pt electrodes (0.785 cm^2 area). The resistance of an YSZ disc of 1.5-mm thickness was measured to be ~50 Ω. The resistance of the sandwich sample was measured to be ~11,000 Ω. From these two values, the resistance of the glass was estimated as ~10,900 Ω. The thickness of the glass layer was 0.5 mm. From these results, the oxygen ion resistivity of the glass is estimated to be $\sim 1.71 \times 10^5$ Ω cm. That is, the ionic resistivity of the glass is orders of magnitude larger than that of YSZ and even larger compared to GDC. This ensures that glass seal-

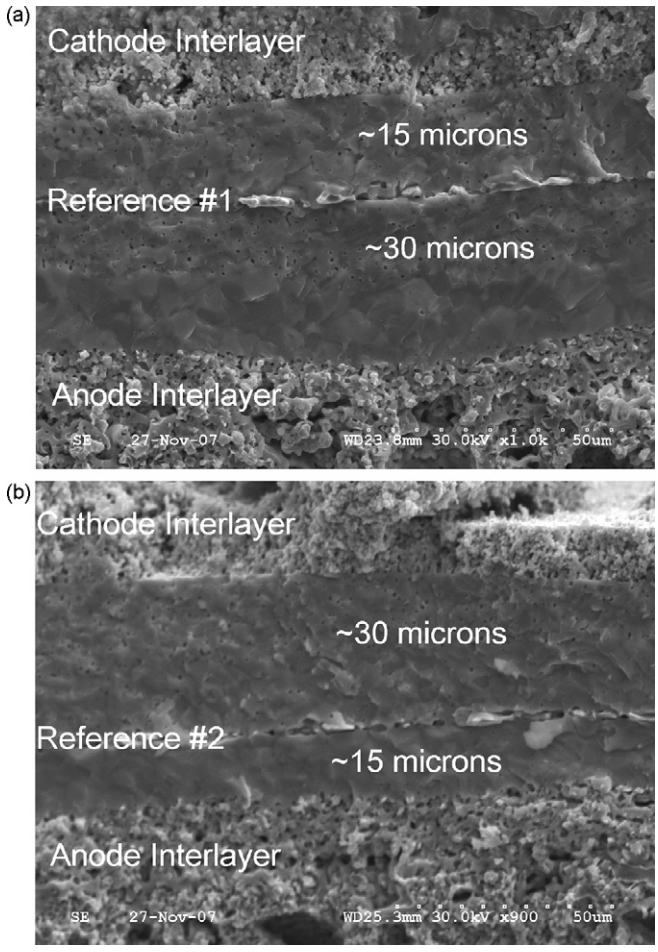

Fig. 5. (a) A scanning electron micrograph (SEM) of the cross-section of a cell showing the anode interlayer, the GDC electrolyte, the cathode interlayer, and the embedded electrode (reference #1) in the GDC electrolyte ~15 μm from the cathode interlayer/GDC electrolyte interface. (b) A scanning electron micrograph of the cross-section of the cell showing the anode interlayer, the GDC electrolyte, the cathode interlayer, and the embedded electrode (reference #2) in the GDC electrolyte ~15 μm from the anode interlayer/GDC electrolyte interface.

ing should virtually shut down any oxygen exchange at the probes.

3.3. Measurement of the conductivity of GDC in air and in a hydrogen containing atmosphere

The resistivity of the GDC bar-shaped sample at 650 °C in air was measured to ~19.5 Ω cm in air. GDC is a predominantly oxygen ion conductor in air at 650 °C. Thus, the measured conductivity is attributed to predominantly oxygen ion conduction. When exposed to hydrogen, the resistance of the sample rapidly decreased and eventually reached a stable value. The resistivity of the sample was measured to be ~4.55 Ω cm. The oxygen ion resistivity is expected to be essentially independent of oxygen partial pressure and thus should be about the same as ~19.5 Ω cm. From these two measurements, the electronic resistivity of GDC at 650 °C in hydrogen is estimated to be ~5.935 Ω cm.

3.4. Measurement of the reduced negative electrochemical potential of electrons, φ

Since GDC is a mixed ionic electronic conductor, the embedded Pt probe can exchange both oxygen ions and electrons, or effectively exchange oxygen. However, because of the high ionic resistivity of the glass used for sealing, exchange of oxygen is suppressed. Thus, the embedded probes should ideally exchange only electrons which facilitates the measurement of φ. Fig. 6 shows the measured voltages between the anode and Ref#2, the anode and Ref#1, and the anode and the cathode as a function of time at 650 °C with 100% H_2 as the anode gas circulated at a flow rate of 300 ml min^{-1}. The data shown in Fig. 6 are after the establishment of steady state. The OCV (anode/cathode) is ~0.85 V. The anode gas was not bubbled through water. However, some H_2O was formed at the anode due to a leakage current through the GDC electrolyte as well as possible leaks through the mica edge seal, and the corresponding p_{O_2} was established at the anode. Fig. 6 shows that the voltages were very stable over the duration of the test. The voltages between the anode and the two reference electrodes were very small (a few mV). In order to determine if this was due to possible shorting of the probes with the anode, test was also conducted with 10% $H_2 + N_2$ as the anode gas circulated at a flow rate of 300 ml min^{-1}. Fig. 7 shows the results of these measurements. In this experiment, the voltages were not stable and this suggests that steady state had not been established. The OCV was between ~0.7 V and ~0.8 V. Note that voltages between the anode and Ref#2 and the anode and Ref#1 are nonzero—they are between about 0.6 V and 0.7 V. This observation suggests that the reference electrodes were not shorted with the anode. The reason for some drop in OCV for times >400 min is not clear. Also, the OCV should be greater than anode/reference electrode voltage, but part of the time it was lower. These discrepancies may be the result of non-steady-state conditions or due to possible incomplete sealing of the probes from the atmosphere. After ~700 min, the anode gas

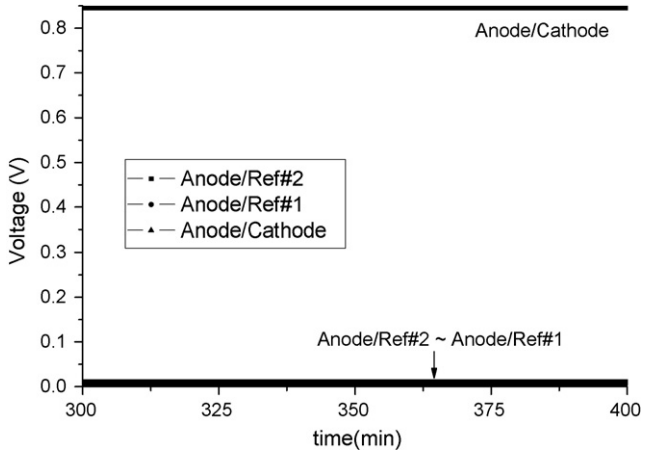

Fig. 6. Measured voltages between the anode and Ref#1 and the anode and Ref#2, and between the anode and the cathode at 650 °C under open circuit condition: fuel, hydrogen; oxidant, air. Note the very small voltages between the anode and the reference electrodes.

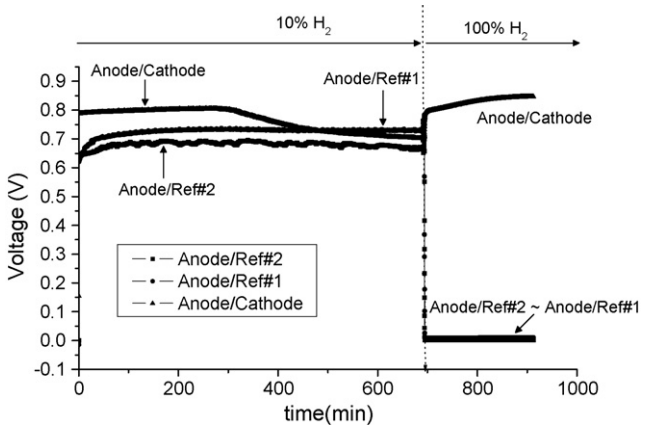

Fig. 7. Similar measurements on a cell with initially 10% H_2 + balance N_2 as the fuel. Relatively high voltages between the anode and the embedded reference electrodes show that the reference electrodes were not physically shorted with the anode. When the anode gas was changed to ~100% H_2, the anode/reference electrode voltages sharply dropped to low values, consistent with the development of significant electronic conduction in the GDC electrolyte.

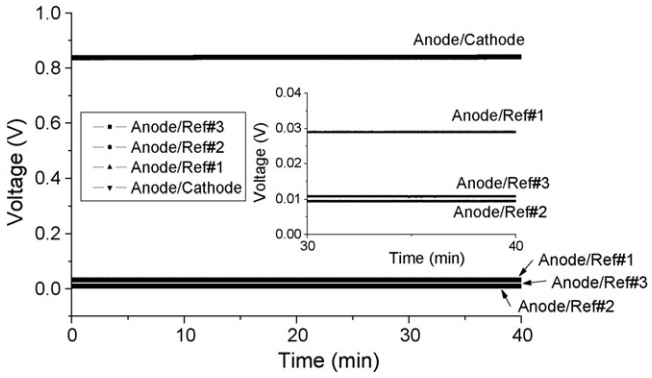

Fig. 9. Measurements of voltages on a cell with three embedded reference electrodes. Measured voltages between the anode and Ref#1, Ref#2, and Ref#3, and between the anode and the cathode at 650 °C under open circuit condition: fuel, hydrogen; oxidant, air. Inset shows an enlarged vertical scale. Note that the voltage between the anode and Ref#1 is the highest (~30 mV). Slightly higher voltage between the anode and Ref#3 than between the anode and Ref#2 is likely experimental scatter.

was switched to 100% H_2. Almost instantaneously the voltages between the anode and Ref#2 and between the anode and Ref#1 dropped to very low values (a few millivolts). The voltage between the cathode and the anode (OCV), by contrast, sharply increased followed by a slow rise to about 0.85 V in about a couple of hours. The observation that the voltage difference ($\Delta\varphi$) between the anode and the reference electrodes is very small is consistent with the development of significant electronic conduction in GDC. Fig. 8 shows the variation of φ through the GDC electrolyte.

Fig. 9 shows $\Delta\varphi$ measurements on a cell with three embedded probes; Ref#3 is ~15 μm from the anode/electrolyte interface, Ref#2 is ~30 μm from the anode/electrolyte interface, and Ref#1 is ~38 μm from the anode/electrolyte interface or ~7 μm from the cathode/electrolyte interface. The anode gas was ~100% H_2. The OCV was ~0.84 V. The measured voltages between the anode and Ref#2 and between the anode and Ref#3 were very small. The measured voltage between the anode and Ref#1 was also small (~30 mV) but still somewhat larger than between the anode and Ref#2 or the anode and Ref#3. The measurements show that φ^{II}, φ^{a}, φ^{ref3}, and φ^{ref2} are about the same, while φ^{ref1} is slightly larger. In order to determine φ^{c}, it was assumed that φ varies linearly between Ref#2 and the cathode/electrolyte interface. Since Ref#1 is symmetrically located between the cathode/electrolyte interface and Ref#2, $\varphi^{c} - \varphi^{ref1}$ should be approximately about the same as $\varphi^{ref1} - \varphi^{ref2}$. The measured open circuit voltage was ~0.84 V and the difference $\varphi^{I} - \varphi^{c}$ is estimated to be ~0.79 V. By contrast, the difference $\varphi^{ref3} - \varphi^{II}$ was measured to be only ~10 mV. Thus, for all practical purposes, the $\Delta\varphi$ across the anode/electrolyte interface ($\varphi^{a} - \varphi^{II}$) is negligible. If we assume $\varphi^{a} - \varphi^{II} \approx \varphi^{ref3} - \varphi^{II}$, then this drop in voltage is ~10 mV, or $\varphi^{a} - \varphi^{II} = r_e^{a} I_e = 10\,\text{mV}$. By contrast, at the cathode, $\varphi^{I} - \varphi^{c} = r_e^{c} I_e = 0.79\,\text{V}$. These results show that the electronic resistance of the cathode/electrolyte interface is much larger than that of the anode/electrolyte interface. Fig. 10 shows a plot of the φ as a function of position in the GDC electrolyte of the cell with three embedded probes.

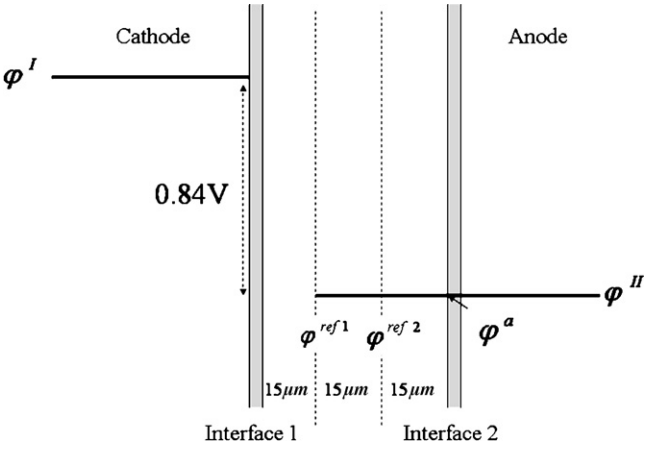

Fig. 8. A plot of the measured φ corresponding to the data given in Fig. 7 with ~100% H_2 as the anode gas.

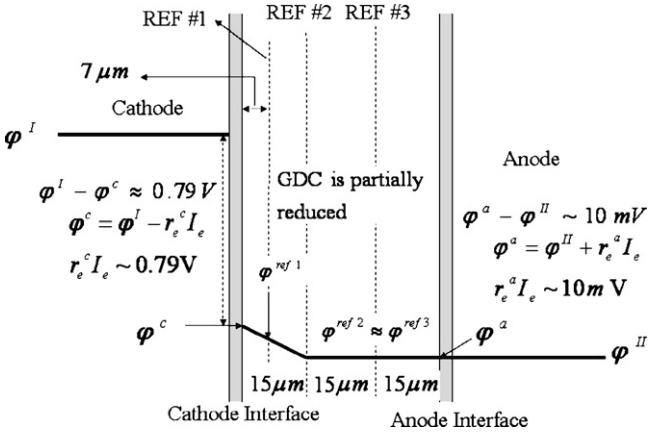

Fig. 10. A plot of the measured φ corresponding to the data given in Fig. 9.

3.5. Estimation of oxygen chemical potential or oxygen pressure using the measurement of φ at open circuit

Voltage vs. current density test was conducted on the cell with three embedded electrodes. The measured voltage vs. current density plot is shown in Fig. 11. From the cell test, the magnitude of the slope is identified with $R_iR_e/(R_i+R_e)$ and is measured as $\sim$0.31 $\Omega\,cm^2$. The open circuit voltage is given by $ER_e/(R_i+R_e)$ and is equal to 0.84 V. Cell voltage was also measured on a GDC-based cell with an YSZ coating which essentially blocks off the electronic current. This cell voltage was measured as 1.05 V at 650 °C, which is assumed to be the Nernst voltage, E. From these measurements, the R_i and R_e are estimated as $\sim$0.39 $\Omega\,cm^2$ and $\sim$1.56 $\Omega\,cm^2$, respectively. From these values, the leakage current is estimated as $|I_i|=|I_e|=0.54\,A\,cm^{-2}$. Using the measured ionic conductivity of GDC at 650 °C of $\sim$0.05 $S\,cm^{-1}$, $(\tilde{\mu}^c_{O^{2-}}-\tilde{\mu}^a_{O^{2-}})/2e$ is estimated as $\sim$0.0474 V, in which the ionic conductivity of GDC is assumed to be independent of p_{O_2}.

In what follows, we will assume that the area specific ionic interface resistance at the anode/electrolyte interface is negligible, that is $r_i^a\approx 0$. The observation that $\varphi^a\approx\varphi^{II}$ also means $r_e^a\approx 0$. In such a case, the $\mu^a_{O_2}-\mu^{II}_{O_2}=\Delta\mu^a_{O_2}\approx 0$. That is, the chemical potential of oxygen nearly equilibrates across the anode/electrolyte interface. Indeed, Raman spectroscopic studies by Mineshige et al. in a GDC electrolyte of 4-mm thickness showed that the chemical potential of oxygen in the electrolyte at the anode/electrolyte interface was essentially the same as in the fuel [22]. This observation shows that indeed $r_i^a\approx 0$ is a reasonable assumption. With this assumption, and the measured φ in the GDC electrolyte, the variation of oxygen chemical potential within the GDC electrolyte can be readily estimated. Fig. 12 shows the plots of φ (measured by embedded probes), $\tilde{\mu}_{O^{2-}}$ (estimated from the ionic conductivity of GDC, the leakage current and the assumption $r_i^a\approx 0$), and $\ln p_{O_2}$ which is a measure of μ_{O_2} (calculated from $\tilde{\mu}_{O^{2-}}$, φ, and the present results showing that $r_e^a\approx 0$). The estimated value of the oxygen partial pressure in the GDC electrolyte just inside the cathode, $p^c_{O_2}$, is estimated to be $\sim 1.99\times10^{-22}$ atm, while that at the cathode is $\sim$0.21 atm; about 21 orders of magnitude drop

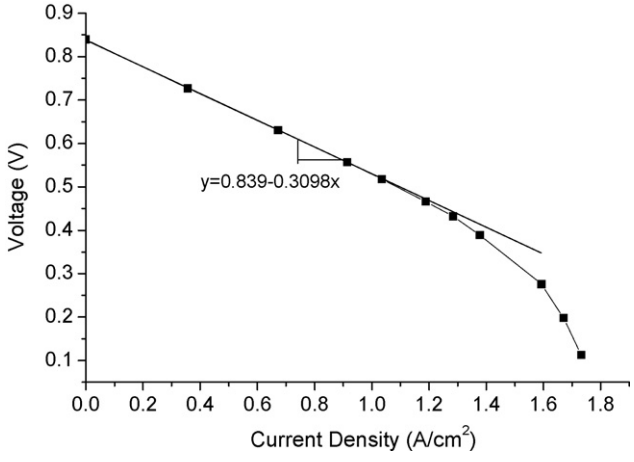

Fig. 11. A performance test at 650 °C on the cell with three embedded reference electrodes.

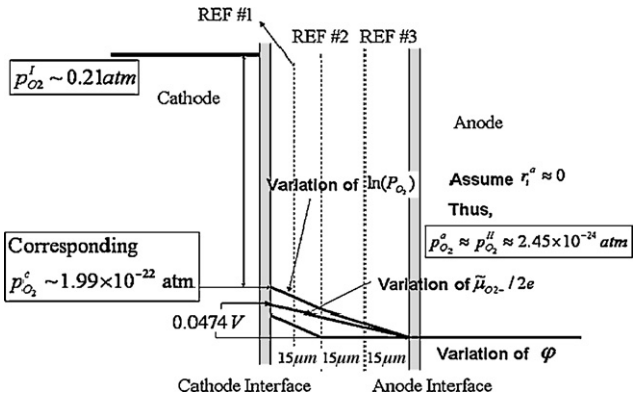

Fig. 12. Plots of φ, $\tilde{\mu}_{O^{2-}}/2e$, and $\ln p_{O_2}$ (or effectively μ_{O_2}) through the GDC electrolyte. Note the sharp drop in p_{O_2} across the cathode/electrolyte interface; $\sim$0.21 atm at the cathode and $\sim 1.99\times10^{-22}$ atm in the GDC electrolyte just across the cathode/electrolyte interface.

in oxygen partial pressure just across the cathode/electrolyte interface. This is quite a remarkable result in that it shows that there is an abrupt change in μ_{O_2} across the cathode/electrolyte interface; that is $\Delta\mu^c_{O_2}=\mu^I_{O_2}-\mu^c_{O_2}\neq 0$, and in fact is rather large. A linear extrapolation of $\ln p_{O_2}$ between ref 2 and ref 1 up to the cathode/electrolyte interface, which is an approximation, was assumed. Even if some nonlinearity is allowed for, it is still clear that there is an abrupt change in μ_{O_2} across the cathode/electrolyte interface. These results also show that the often made assumption of the equilibration of chemical potential of oxygen across a gas/solid interface when there is a net, nonzero $\Delta\mu_{O_2}$ across the membrane, is generally not true. We have also seen that $\Delta\varphi^c=\varphi^I-\varphi^c\approx 0.79$ V. This means the electronic area-specific resistance at the cathode/electrolyte interface is given by $r^c_e=\Delta\varphi^c/|I_e|$ or $r^c_e\approx 0.79/0.54\,\Omega\,cm^2$ or $\sim$1.463 $\Omega\,cm^2$.

Now the $R_i\approx 0.39\,\Omega\,cm^2$ and $r_i^a\approx 0\,\Omega\,cm^2$. From the measurement of conductivity of GDC in air, the estimated value of the electrolyte ionic area-specific resistance is $r_i^{el}\approx 0.09\,\Omega\,cm^2$. From these measurements, since $R_i=r_i^c+r_i^{el}+r_i^a$, the area-specific cathode/electrolyte ionic interface resistance is estimated as $r_i^c\approx 0.3\,\Omega\,cm^2$. The performance of GDC as a good electrolyte for SOFC applications is thus attributed to the large value of r_e^c, electronic resistance at the cathode/electrolyte interface, which leads to moderately high ionic transference number for the cell. The present results also thus suggest that virtually all of the GDC electrolyte thickness even in a thin electrolyte anode-supported SOFC is a mixed ionic electronic conductor and much of the voltage drop, $\Delta\varphi$, and much of the chemical potential of oxygen drop, $\Delta\mu_{O_2}$, drop across the cathode/electrolyte interface.

In the work by Mineshige et al., analysis of their data was made under the assumption that the μ_{O_2} equilibrated across both cathode/electrolyte and anode/electrolyte interfaces; that is $\mu^c_{O_2}\approx\mu^I_{O_2}$ and $\mu^a_{O_2}\approx\mu^{II}_{O_2}$ [22]. Their experimental results on the anode side were in agreement with the assumption $\mu^a_{O_2}\approx\mu^{II}_{O_2}$. However, examination of their Fig. 5 shows that $\mu^c_{O_2}\neq\mu^I_{O_2}$ and that $\mu^c_{O_2}<\mu^I_{O_2}$, and thus not in agreement with the assumption $\mu^c_{O_2}\approx\mu^I_{O_2}$ made in their work. That is,

in their work also there was a sharp drop in μ_{O_2} across the cathode/electrolyte interface, which is not in agreement with their (and commonly made) assumption of the equilibration of chemical potential across the gas/solid interface. However, the abrupt change in μ_{O_2} observed in their studies and in the present work is in complete accord with the present work and analysis presented previously [7].

4. Summary

Anode-supported cells with GDC electrolyte of thickness ~45 μm, LSC + GDC cathode interlayer, Ni + GDC anode interlayer, and Ni + YSZ anode support were fabricated with Pt probes embedded within the GDC electrolyte. Up to three Pt probes were embedded within the electrolyte. The probes were sealed off from the atmosphere using a glass impermeable to oxygen. Voltages, $\Delta\varphi$, between the anode and the embedded probes and between the anode and the cathode were measured at 650 °C with air circulated past the cathode and hydrogen past the anode. It was observed that there was negligible voltage difference between the anode and the embedded reference electrodes, and much of the voltage dropped across the cathode/electrolyte interface. This drop is attributed to a large electronic area-specific resistance, r_e^c, across the cathode/electrolyte interface. Based on these results, the chemical potential of oxygen, μ_{O_2}, through the GDC electrolyte was mapped out as a function of position. The results show that much of the chemical potential of oxygen, $\Delta\mu_{O_2}$, also drops across the cathode/electrolyte interface. The present results show that in an SOFC made with a mixed ionic electronic conducting ceria electrolyte, such as GDC, only an extremely thin layer at the cathode/electrolyte interface functions as an electrolyte.

Acknowledgement

This work was supported by the U.S. Department of Energy under Grant Number DE-FG02-06ER46086.

References

[1] M.H. Hebb, J. Chem. Phys. 20 (1952) 185.
[2] L. Heyne, Mass Transport in Oxides, vol. 296, NBS Special Publication, 1968, p. 149.
[3] C. Wagner, Prog. Solid-state Chem. 10 (1) (1975) 3–16.
[4] J.S. Kirkaldy, D.J. Young, Diffusion in the Condensed State, The Institute of Metals Publication, London, 1987.
[5] R.D. Armstrong, M. Todd, in: P.G. Bruce (Ed.), Solid State Chemistry, Cambridge University Press, Cambridge, UK, 1995.
[6] D. Kondepudi, I. Prigogine, Modern Thermodynamics, Wiley, New York, 1998.
[7] A.V. Virkar, J. Power Sources 147 (2005) 8.
[8] A.V. Virkar, J. Electrochem. Soc. 138 (5) (1991) 1481–1487.
[9] A.V. Virkar, J. Power Sources 172 (2007) 713–724.
[10] I. Reiss, Mater. Sci. Eng. B: Solid B12 (1992) 351.
[11] N.S. Choudhury, J.W. Patterson, J. Electrochem. Soc. 117 (11) (1970) 1384.
[12] N.S. Choudhury, J.W. Patterson, J. Electrochem. Soc. 118 (9) (1971) 1398.
[13] S. Yuan, U. Pal, J. Electrochem. Soc. 143 (10) (1996) 3214.
[14] P. Soral, U. Pal, W.L. Worrell, J. Electrochem. Soc. 145 (1) (1998) 99.
[15] R. Singh, K.T. Jacob, J. Appl. Electrochem. 33 (2003) 571.
[16] A. Sawata, K. Tsuneyoshi, J. Mizusaki, H. Tagawa, Solid State Ionics 40/41 (1990) 415.
[17] S.H. Chan, X.J. Chen, K.A. Khor, J. Appl. Electrochem. 31 (2001) 1163.
[18] T. Suzuki, P. Jasinski, H.U. Anderson, F. Dogan, J. Electrochem. Soc. 151 (10) (2004) A1678.
[19] C. Rosenkranz, J. Janek, Solid State Ionics 82 (1995) 95.
[20] J. Mizusaki, Solid State Ionics 82 (1995) 95.
[21] D.M. Reed, H.U. Anderson, W. Huebner, J. Electrochem. Soc. 143 (5) (1996) 1558.
[22] A. Mineshige, T. Taji, Y. Muroi, M. Kobune, S. Fujii, N. Nishi, M. Inaba, Z. Ogumi, Solid State Ionics 135 (2000) 481.